C.Bedon, G.Rinaldin, M.Fragiacomo (2015). "Non-linear modelling of the in-plane seismic behaviour of timber Blockhaus log-walls", Engineering Structures, 91(5): 112-124.

Non-linear modelling of the in-plane seismic behaviour of timber 'Blockhaus' log-walls

Chiara Bedon*[1], Giovanni Rinaldin[2] and Massimo Fragiacomo[3]

Abstract

This paper investigates the non-linear modelling of the cyclic behaviour of *Blockhaus* timber log-walls under in-plane lateral loads. The structural behaviour of *Blockhaus* log-walls in the examined loading condition strictly depends on the geometry – thus on the deformability and ultimate resistance – of the adopted corner joint, namely the joint between perpendicular log-walls. The presence of metal fasteners is in fact minimized and the structural interaction between the basic timber components is provided by simple mechanisms such as notches, tongues and grooves, multiple surfaces in contact. In this paper, a computationally effective FE-model is developed, in order to predict the cyclic behaviour of an entire *Blockhaus* log-wall once the cyclic behaviour of the adopted corner joint is known. The model uses non-linear hysteretic springs to describe the joint behaviour, where all typical features such as pinching behaviour, strength and stiffness degradation can be considered. By comparing the numerical and the experimental predictions of the cyclic response of full-scale *Blockhaus* log-walls, a general good agreement is found. Simulations confirmed the high flexibility of the studied structural systems, as well as the significant effect of possible openings such as doors and windows on their global resistance to in-plane lateral loads. In conclusion, the presented study confirmed that the proposed modelling approach can be used to estimate the load-carrying capacity and vulnerability to seismic events of *Blockhaus* shear walls, and that the same model could be extended to full *Blockhaus* buildings.

Keywords: *Blockhaus* timber log-walls; non-linear model; full-scale tests; joint behaviour; hysteresis law

[1] Ph.D., Researcher. Department of Engineering and Architecture, University of Trieste, Piazzale Europa 1, 34127 Trieste, Italy. Corresponding author. E-mail: bedon@dicar.units.it. Phone: +39 040 558 3837. Fax: +39 040 558 3580.
[2] Ph.D., Research Fellow. Department of Architecture, Design and Urban Planning, University of Sassari, Piazza Duomo n.6, 07041 Alghero (SS), Italy. E-mail: grinaldin@uniss.it
[3] Associate Professor. Department of Architecture, Design and Urban Planning, University of Sassari, Piazza Duomo n.6, 07041 Alghero (SS), Italy. E-mail: fragiacomo@uniss.it

1. Introduction

The paper investigates the seismic cyclic response of *Blockhaus* shear walls. The typical *Blockhaus* (or log-haus, log-house, log-home, etc.) system consists of a series of timber logs stacked horizontally one upon each other and interacting together by means of traditional and ancient connections based on carvings, notches and contacts of multiple timber surfaces. The presence of metal fasteners and steelwork is minimized in these structural systems, with significant advantages in terms of cost reduction during production (e.g. carving of timber logs) and assembling on the building site. Nevertheless, due to the lack of mechanical fasteners, the structural behaviour of *Blockhaus* buildings is complex to describe rigorously.

The seismic characterization of these construction systems represents a topic of great interest for researchers and designers. *Blockhaus* buildings are in fact widely popular and largely used in practice for the construction of wooden houses, so that the average annual turnover of constructed log-haus buildings can be directly compared to that of timber-framed structures [1]. Although timber log structures have been originally manufactured in forested areas like Scandinavia, Russia, Eastern Europe and North America, especially for buildings located in rural and suburban environments, this structural system is used nowadays for the construction of residential and commercial buildings (e.g. hotels, schools, etc.) in various regions of Northern and Central Europe, South Africa, and earthquake-prone regions such as Japan and the Mediterranean (e.g. [1][2][3][4][5]).

Scarce contributions however are available in literature for these timber-log structural systems. Hirai et al. [6], for example, focused on the assessment of the damping capacities of timber log-walls under in-plane lateral loads, and experimentally estimated an average static friction coefficient of 0.67. Further friction experiments on small log-wall specimens and simplified numerical studies of *Blockhaus* structural systems under seismic loads were presented in [7][8]. The seismic behaviour of a full-scale *Blockhaus* building was investigated in [8] by means of a simplified numerical model consisting of a series of rigid beams linked together by springs. Those springs were able only to partially describe the effective interaction between multiple logs in contact as, for example, friction at the interface of the different interaction surfaces was ignored. At the same time, the mechanical behaviour of each spring was calibrated to a constant shear stiffness value obtained from cyclic experiments performed on small corner joints.

Thus, possible overturning effects and detachments between logs, as well as the influence of vertical pre-compressive loads on the global response of each main wall, was not taken into account. Finally, the possible strengthening and stiffening contribution of internal orthogonal walls (e.g. intermediate restraints) was neglected.

Further full-scale tests and extensive small-scale experiments were recently performed respectively on *Blockhaus* shear walls and single *Blockhaus* corner joints also in [9][10][11]. In these works, both the monotonic and the cyclic structural behaviour of timber-logs having various geometrical properties were investigated. In [12], full 3D Finite-Element (FE) models with solid elements, calibrated to several types of experiments performed on small *Blockhaus* components (e.g. small log specimens tested to assess the static friction coefficient, or typical corner joints loaded perpendicular to the grain, to estimate the ultimate compressive strength) and full-scale log-wall specimens, were presented to investigate the monotonic behaviour of timber log-walls subjected to in-plane lateral loads. The advantage of the FE-numerical models presented in [12], quite different from the numerical approach presented in [8], is given – once known the friction coefficient and the mechanical properties of timber – by the accurate description of multiple interactions between logs and surfaces, which makes testing single corner joints not necessary for the prediction of the entire log-wall behaviour. Conversely, full 3D FE-models are unavoidably associated to high modelling and computational cost, and therefore are generally unsuitable to describe whole log-haus structural systems and buildings, and especially their seismic behaviour. As a result, a simplified computationally efficient modelling approach able to preserve the accuracy of full 3D FE-models and correctly reproduce the structural interaction between the *Blockhaus* components is necessarily required.

In this paper, past experimental results obtained from cyclic tests recently performed on six different types of *Blockhaus* shear walls and further small corner joints are firstly described [9][10][11][12]. As shown, when these log-walls are subjected to in-plane lateral loads, the timber-timber connections ensure significant flexibility of the structural system and enable the attainment of large displacements. At the same time, the shear strength of log-walls under in-plane lateral loads strictly depends on the number of intersections between the main wall and perpendicular walls, as well as on the geometry – thus on possible small gaps and on the resisting surfaces – of the adopted connection details.

Unlike in [8][12], a novel, computationally efficient numerical approach is then presented. Its efficiency derives from the basic phenomenological approach adopted for the mechanical characterization of its components, as well as the interaction between them once assembled together. Non-linear springs, appropriately calibrated to test results obtained from *Blockhaus* corner joints under cyclic loads [10, 11], are in fact used to properly reproduce the shear and the compressive strength of half timber logs, which are modelled instead as rigid components. In the same springs, possible friction mechanisms occurring along the contact surfaces of logs are also taken into account.

As shown, a general good agreement is found between full-scale test results and the corresponding numerical simulations, both for log-walls without openings or with door and window openings. As expected, the FE-models confirmed the high flexibility of the studied log-walls, but also the significant influence of possible openings on their global structural response. Parametric studies carried out on log-walls with various overall dimensions are also presented. The proposed modelling approach cannot take into account possible effects deriving from changes in moisture, shrinkage and swelling. However, based on the discussed studies, it is expected that the same method could be further extended and applied to full *Blockhaus* buildings, in order to properly assess their vulnerability to seismic events.

2. Past experiments on *Blockhaus* log-walls and joints under in-plane lateral loads

2.1. Full-scale specimen configurations, test protocol and results

Six different types of *Blockhaus* shear walls were experimentally investigated in [9, 12]. The typical specimen consisted of an $H_w \times L_w$ main log-wall and two $H_c \times L_c$ orthogonal log-walls able to provide appropriate continuous lateral supports (Fig. 1).

The main characteristic of these systems is that the shear walls are obtained by positioning horizontally a series of *b*-wide and *h*-deep, C24 spruce timber logs [13] with specific cross-sectional features. Examples are provided in Fig. 2 for 'Tirol' and 'Schweiz' profiles, currently in use at Rubner Haus AG SpA [1] and characterized by the presence of $\approx$ 10×10mm tongues and grooves able to improve interlock and friction properties between their top and bottom contact surfaces.

Once the main log-wall is assembled, the structural interaction with the intercepting log-walls is ensured by appropriate corner joints. Various typologies of carpentry joints have been developed over the last decades. Among them, the 'Standard' saddle notch corner (Fig. 3a) represents one of the earliest forms of intersections for *Blockhaus* structural systems. The timber logs are notched only near the ends - both at the top and at the bottom of their nominal cross-section - so that each row of log interlocks and passes through. In the case of 'Tirolerschloss' joints (Fig. 3b), conversely, the structural interaction between logs is provided by appropriate dovetails and angular cuts at the log ends.

The main differences between the six tested full-scale log-walls were given by the overall dimensions $H_w \times L_w$ of each specimen, as well as by their cross-sectional properties (Fig. 2) and by the adopted corner joints (Fig. 3). Each of the tested specimens was in fact restrained at its lateral ends by orthogonal log-walls characterized by $H_c \equiv H_w$ height and L_c= 0.9m total length (Fig. 1). Nominal dimensions of the tested specimens are summarized in Tables 1 and 2, together with the main results derived from cyclic experiments [9, 12].

In the case of one specimen only (HW01, Table 1), the geometry of the main log-wall was characterized by the presence of two openings (Fig. 4): a door (1.12m wide × 2.15m high) and a window (1m wide × 1.5m high) 0.55m-spaced from the vertical mid-point axis of the $H_w \times L_w$ log-wall. When openings like doors and windows are present in *Blockhaus* log-walls manufactured by [1], the structural interaction between the interrupted logs is only ensured by hollow section steel profiles introduced along the vertical edges of the openings, within a notch cut (details of Figs.4b-4c). Although these small profiles can offer increased bending stiffness of the studied log-walls against out-of-plane deflections, as recently demonstrated in [14, 15], they are not rigidly connected to the adjacent timber logs. As a result, their structural efficiency in presence of in-plane lateral loads is almost null.

According to the setup schematized in Fig.1d, each full-scale specimen was subjected to quasi-static cyclic tests, in order to assess the shear resistance and flexibility under in-plane lateral loads, as well as to estimate the possible decrease of the resistance and the damping properties after a certain number of cycles. The experiments were performed at CNR Ivalsa (specimens W01 and W05 [12]) and University of Trento

(specimens W02, W03, W04, HW01 [9]), respectively. In both cases, controlled temperature and relative humidity conditions (T=20 (± 2) °C and RH=65 (± 5) %) were guaranteed.

The investigated shear walls were rigidly attached to the foundation by means of metal connectors (namely 3mm thick steel angle brackets positioned as shown in Fig.1d, and connected to the bottom timber log and to the ground by means of metal nails and M10 bolts, respectively [12]), as usually done in practice for *Blockhaus* systems installed by Rubner Haus [1]. All the specimens were preliminarily vertically pre-compressed and subjected to a nominal compressive distributed load of q= 10kN/m representative – being *Blockhaus* structural systems generally used in practice for buildings up to two levels – of permanent and accidental design loads deriving from the roof, the second level log-wall and second level floor in a seismic loading combination [17]. Only for the specimen W03, the pre-compressive load was halved (q= 5kN/m). The uniform distribution of the applied loads on the specimens was ensured by an upper metal profile rigidly connected to the horizontal jack head and to the upper side of the top timber logs (Fig. 1d). In each specimen, additional 10mm diameter steel cables were also attached to the ends of the upper log (Fig.1d) to avoid the possible overturning of the log-walls during the in-plane cyclic experiments. Based on recommendations of EN 12512:2003 [16], the in-plane cyclic lateral force was then introduced at the top-end surface of each specimen via a hydraulic jack equipped with a load cell connected to a reaction frame (Fig.1d).

The amplitude of cycles was estimated based on a reference slip δ_y= 5mm (≈ H_w/590) and δ_y= 10mm (≈ H_w/280) for the experiments on specimens W01, W05 and W02, W03, W04, W06, HW01 respectively. The displacement rate was initially set to 0.05mm/s, and gradually increased up to 0.5mm/s at the attainment of large horizontal displacements. All the tests were stopped at the attainment of a maximum lateral displacement at the top log δ_{max}= 80mm (≈ H_w/36, for W01 and W05 specimens) and δ_{max}= 100mm (≈ H_w/28, for W02, W03, W04 and HW01 specimens).

The full-scale experiments showed an overall appreciable dissipative capacity and high flexibility of the tested log-walls. Comparative plots are proposed in Sections 3.4 (Fig.11) and 3.6 in the form of horizontal in-plane load V versus the top lateral displacement δ curves. Further test results are proposed also in Tables 1 and 2, in terms of maximum attained lateral displacement δ_{max} and shear force V_{max}, expected characteristic

failure load V_k, equivalent damping ratio ν_{eq} derived from various amplitudes of imposed displacement δ (with calculations referred to the first full cycle for each displacement δ) and friction coefficient μ.

The in-plane lateral response of the studied systems, as also highlighted in [12], directly depends on the adopted corner joints (e.g. number of interceptions and resisting contact surfaces), as well as on friction mechanisms deriving from possible sliding among the overlapping logs. The Eurocode 5 for timber structures [18], for example, estimates the expected characteristic failure load V_k as the minimum failure load associated to a compressive ($V_{k,comp}$) or a shearing collapse mechanism ($V_{k,shear}$):

$$V_k = \min\left(V_{k,comp}, V_{k,shear}\right) = \min\begin{cases} V_{k,comp} \le k_{c,90}\, f_{c,90,k}\, n_i\, A_{ef} & (1a) \\ V_{k,shear} \le \dfrac{2}{3}\, f_{v,k}\, n_i\, A_{shear} & (1b) \end{cases}$$

In Eqs.(1a) and (1b), n_i represents the number of intercepting orthogonal walls; A_{ef} and A_{shear} are the corresponding resisting surfaces; $f_{c,90,k}$ and $f_{v,k}$ denote the characteristic compressive strength perpendicular to grain and the characteristic shear strength of C24 spruce, respectively [13]. The coefficient $k_{c,90}$ given by Eq.(2) [18]:

$$k_{c,90} = \left(2.38 - \frac{l}{250}\right)\left(1 + \frac{h}{12l}\right), \qquad (2)$$

finally, takes into account the specific loading configuration for members on resting supports under compression perpendicular to the grain, l being the contact length and h the timber-log depth respectively (dimensions in mm).

As highlighted in Table 1, only for specimens W01 and HW01, the maximum shear load V_{max} obtained at the end of the experiments resulted lower than the corresponding predicted characteristic resistances V_k. This effect could derive from lower mechanical properties of timber composing the specimens, compared to nominal characteristic values derived from [13] for C24 spruce. In any case, it should be noticed that these tests were stopped at the attainment of a maximum lateral displacement δ_{max}= 80mm, and no sign of damage was noticed in the log-walls. In the case of specimen HW01, the presence of openings markedly affected the structural response of the tested wall, especially in terms of global flexibility, due to the unrestrained portion of logs between the door and the window. Since Eqs.(1a) and (1b) do not properly consider possible

openings - being the shearing collapse load V_k dependent on the number of interceptions between the main wall and the orthogonal walls only - it is clear that the effective geometry and position of openings should be properly taken into account in the design and verification of these structural systems.

Compared to other timber structural systems (Table 2), all the investigated specimens showed large damping capacities, being their average equivalent viscous damping ratio ν_{eq} [16] calculated at a top lateral displacement δ= 80mm equal to ≈ 0.12. It should be noticed that full-scale cyclic experiments performed on light-frame timber shear walls [19] resulted in an equivalent damping ratio $\nu_{eq} \approx 0.14$. Further experiments carried-out by Vasconcelos et al. [20] on timber-framed shear walls with brick masonry infill provided comparable damping capabilities ($\nu_{eq} \approx 0.15$), especially if compared to test results of *Blockhaus* specimens W01-W05 without openings. In the case of specimen HW01, although the presence of openings resulted in an almost local failure, an appreciable damping capacity was obtained.

Finally, an average friction coefficient $\mu \approx 0.4$ was found, with higher friction values for the W03 (e.g. lower pre-compressive level) and W04 (e.g. 'Schweiz' logs) specimens.

2.2. *Blockhaus* corner joints

Further quasi-static monotonic and cyclic experiments were performed on single *Blockhaus* 'Standard' and 'Tirolerschloss' corner joints [10, 11], in order to properly assess their structural behaviour under in-plane lateral loads and the effects of various influencing parameters (e.g. pre-compression level, type of joint). A total number of 19 experiments (including 4 pilot experiments and 4 +1 monotonic/cyclic tests for each joint type) were carried out. The experiments generally confirmed a rather stable behaviour for all the series of specimens [10, 11], and also provided rather good agreement with past 3D numerical models [12]. Three different types of specimens (N01, N02, N03), respectively representative of (i) a 'Standard' joint with 'Tirol' cross-section, (ii) a 'Standard' joint with 'Schweiz' cross-section and (iii) a 'Tirolerschloss' joint with 'Tirol' cross-section were in fact investigated (Fig. 5). All the specimens consisted of four timber logs having a total length of 0.5m and representative of a typical interception between a main log-wall (two logs) and an orthogonal log-wall (two logs), as schematized in Fig.5b.

An appropriate self-made test apparatus was used, in order to obtain the desired loading and boundary conditions. In accordance with the full-scale test setup discussed in Section 2.1, the 'main log-wall' was subjected to a vertical pre-compressive load of 10kN/m, properly introduced by means of elastic springs (Figs.5a-5b). Thermoplastic layers (Polizene®, [21]) able to prevent friction mechanisms among the steel-to-timber contact surfaces were also used, and interposed between the corner joints and the setup apparatus (Fig.5a). The lower timber log of each main log-wall (Fig.5b, log #1) was rigidly connected to its base, so that the translation due to the applied in-plane lateral loads could be prevented, whereas the in-plane horizontal load was applied to the upper timber log (Fig. 5b, log #2).

Cyclic experiments were performed in accordance with [16]. The reference slip was set to δ_y= 5mm, whereas the displacement rate was set to 0.1mm/s for the initial cycles and gradually increased up to 0.5mm/s at the attainment of large displacements. During the experiments, the in-plane lateral displacement δ (point A of Fig.5b), the vertical uplift u_y of the loaded timber logs (point C of Fig.5b) and the rotation φ_z of the orthogonal logs (point B of Fig.5b) were continuously monitored.

All the experiments were stopped at the attainment of the failure condition for each joint (Figs. 5c-5d). The failure of each specimen was defined from three conditions, whichever occurs first: (i) collapse of the timber logs (namely, a brittle shear failure mechanism at the end of the main logs, or crushing in the notches of the orthogonal logs); (ii) attainment of a maximum lateral displacement of 30mm, and (iii) attainment of a maximum in-plane load equal to 80% of the maximum load V_{max} obtained from the V-δ cyclic tests, in the decreasing path.

Tests performed on single joints generally confirmed the high flexibility and damping capacities of this connections. At the same time, the tests emphasized the influence on their overall predicted behaviour deriving from small gaps (0.5mm-1mm) within the joint themselves, as also discussed in [12], since directly responsible of sliding occurring between the overlapping logs.

'Standard' specimens N01 and N02 showed the typical hysteresis curves of timber joints, that is pinched cycles with almost vertical curves in the unloading phases. In terms of equivalent viscous damping ratios [16], almost stable values were obtained for 'Standard' joints (ν_{eq}= 0.179 and 0.199 for specimens N01 and N02 at δ= 20mm). These specimens failed due to local crushing in the region of contact between the loaded

logs and the orthogonal logs (Fig. 5c), and for this reason the test on joint N01 attained a lower maximum displacement, compared to joints N02 and N03.

In the case of the 'Tirolerschloss' specimen N03, a significantly higher damping ratio $\nu_{eq} \approx 0.276$ was obtained, due to the high energy dissipation offered by rectangular hysteresis loops typically manifested by this typology of corner joint [10, 11]. Although the joint failed due to the opening of pronounced cracks near the end-protrusions of the logs (Fig. 5d), specimen N03 demonstrated high dissipative capacity and an almost regular cyclic behaviour, compared to 'Standard' specimens.

Compared to data collected in Table 2, the experiments carried out on single joints further confirmed the correlation between their estimated damping capacity and the measured sliding. It should be noticed that during the full-scale cyclic experiments, the imposed top-lateral displacement δ was almost equally distributed along the height of the log-walls, thus resulting in very small amplitudes of sliding in each joint, compared to the experiments on N01, N02 and N03 joints.

3. Numerical investigation

The aim of this contribution is the development of a computationally effective finite-element (FE) model for accurate seismic analyses of *Blockhaus* subassemblies and buildings. As discussed in Section 2, the cyclic behaviour of typical log-walls and joints used in the *Blockhaus* system is rather complex to describe correctly, being characterized by pinching, stiffness and strength degradation. The contribution of friction and localised crushing at the interface between logs are also important phenomena that affect the global nonlinear monotonic and cyclic behaviour. To account for all these phenomena, a full 3D numerical model using solid finite elements was implemented in ABAQUS/Standard [22] in a previous paper [12]. Although this model was able to predict with excellent accuracy the experimental monotonic nonlinear behaviour of *Blockhaus* log-walls and single joints, the model was computationally too cumbersome and could not be used to predict the cyclic behaviour of subassemblies and entire *Blockhaus* buildings. On the other hand, simplified wall schematizations such as those presented in [8] are not able to capture typical features such as pinching, strength and stiffness degradations, and need experimental results of the actual full-scale log-wall subjected to cyclic load for a proper calibration.

3.1. Numerical modelling

The FE-model proposed in this paper is geometrically simpler but structurally more efficient than the full 3D model presented in [12]. Each *Blockhaus* wall is described as a series of rigid beams - representative of the main $b \times h \times L_w$ timber logs - connected at their ends by non-linear spring elements acting in their axial (Y direction) and transversal (shear – X direction) degrees of freedom (Fig. 6). Every spring represents the mechanical cyclic behaviour of a single carpentry joint.

The main advantage of this schematization is the computational efficiency due to the adopted phenomenological approach: each non-linear spring represents the shear (sliding in X direction) and the compressive (springs in Y direction) strength of one-half of each log, which is modelled instead as rigid. Axial and shear DOFs of the spring have a piece-wise cyclic characterization, as displayed in Fig. 7, and are independent of each other.

The shear law is symmetric, whereas the axial law represents the contact behaviour in compression in a lumped way. The compressive resistance of each spring (branch #10 of Fig.7b) is estimated as the characteristic compressive strength $f_{c,90,k}$ of timber in the direction perpendicular to grain, multiplied by the top/bottom contact surface of a single orthogonal log ($90 \times 600 mm^2$ contact area, based on the nominal dimensions of specimens given in Table 1 and Figure 1). Conversely, in tension the axial spring has a very low stiffness to represent the uplift and possible separation of one beam from another (branch #1 in Fig. 7b).

The shear hysteretic law has a tri-linear backbone curve and specific unloading-reloading paths from the elastic (before F_{el} in Fig. 7a, branches #1 and #10 on the backbone curve) and the inelastic phases (branches #2, #3, #20 and #30 on the backbone curve) respectively. The unloading paths in elastic phase, displayed in Fig. 7a with dashed lines, are characterized by two branches: the first one (branch #11) leads to a null strength with a stiffness k_{sc} times the elastic one (see Table 3 for the implemented values), whereas the latter one (branch #12) leads to a percentage of the maximum displacement reached on branch #10. The reloading path in Fig. 7a in the elastic phase, finally, is symmetric compared to the unloading path (branches #110 and #120).

The unloading and reloading paths are composed by four branches each (#4, #8, #6, #40 and the symmetric ones), which schematize the pinching effect in plastic field, for unloading starting from branches #2 or #3

and #20 or #30. The branch #4 has a stiffness k_{sc} times the elastic one, while the slope of branch #8 is a fraction of the elastic one. The branches #40 and #5 are characterized by a degraded elastic stiffness: the degradation is linear and starts once F_{el} is attained; the ultimate value is used at the ultimate displacement and is equal to k_{deg} times the elastic stiffness. Finally, the presented law implements also a strength degradation through an additional displacement at reloading (δ_E in Fig. 7a), which is proportional to the dissipated energy in the last full reversed cycle and can be set through the parameters α and γ in Table 3. Further details can be found in [23]. The axial relationship needs only three parameters to be defined: tension and compression stiffnesses, and the ultimate compressive displacement, so that possible crushing mechanisms in the carpentry joints could be taken into account. The shear relationship needs 14 parameters to define the backbone curve and the unloading-reloading paths. A list of parameters for the shear law with a brief description is given in Table 3. The first five and the d_u parameters define the symmetric backbone curve, while k_{sc}, R_c, S_c and k_5 describe the unloading and reloading paths. α, γ and k_{deg} are related to the strength degradation and are used to calibrate the strength loss and the stiffness degradation laws in [23]. The parameter *Gap*, finally, specifies the gap opening (positive value) in the corner joint. In this work, in accordance with [12], average gap amplitude of 1mm was taken into account. All the parameters for the shear law were evaluated with the software So.p.h.i. [24], as discussed in a subsequent paragraph.

3.2. Dynamic friction effect

The effect of dynamic friction was also included in the model, since it provides an additional strength contribution to each shear spring given by:

$$F_f = C_f \cdot N \tag{3}$$

In Eq. (3), N signifies the resultant axial (vertical) force in the spring at the current analysis step; C_f denotes the dynamic friction coefficient and F_f signifies the dynamic friction force applied in the shear direction of the spring.

The cyclic behaviour of friction effect is showed in Fig. 8. The stiffness k_f in Fig. 8 was set to 10 times the shear stiffness of the connector (branch #1 in Fig. 7). According to Eq. (3), the increase in shear strength due to friction directly depends on the axial force acting in the spring. Finally, the dynamic friction coefficient C_f

has been assumed equal to μ= 0.4, in accordance with the average friction coefficient derived from full-scale cyclic experiments (Table 2).

3.3. Calibration of the springs

The springs were calibrated on the experimental results obtained from single carpentry joints under in-plane cyclic loads [10, 11] presented in Section 2.2.

The calibration was performed with the software So.ph.i. v.4.5 [24], which automates the calibration of the backbone curve according to EN 12512 [16]. The software operates by comparing the force-displacement cycles from the test with the numerical approximating ones, obtained with the relationships described in [23] by imposing the experimental displacements. The discrepancy between experimental and numerical approximating curves is then evaluated in terms of total energy.

In this work, a 5% maximum difference on their final values was considered acceptable. An optimization method was used, by changing the parameters related to the hysteretic cycles until a 5% difference was attained. The springs were calibrated for each experimental test. The obtained optimized parameters are presented in Table 3 for each corner joint, while the corresponding experimental (E_{exp}) and numerical approximating (E_{num}) energy values of specimens N01, N02 and N03 are listed in Table 4. The calibration of the springs on the experimental cyclic results are also displayed in Fig. 9, as in-plane shear load V versus lateral (shear) displacement δ, for the three corner joints. These joint calibrations were then used to describe the cyclic behaviour of 'Standard' and 'Tirolerschloss' joints within the full-scale log-wall specimens.

3.4. Numerical analyses of *Blockhaus* walls without openings

Non-linear static analyses under cyclic loading were performed on the full-scale *Blockhaus* walls described in Section 2 using the proposed FE-modelling approach. Firstly, specimens W01-W05 without openings were analysed. Each FE-model was obtained by assembling a series of horizontal rigid beams and non-linear springs, and then analysed under cyclic loads by imposing the experimental displacement time-history (Section 2.1) at the top log of each wall.

The non-linear springs were calibrated on the experimental cyclic tests carried out on the single corner joints (Section 2.2), depending on the joint typology adopted in the corresponding full-scale specimens (more specifically: specimen N01 in walls W01, W02 and W03; specimen N02 for W04; and specimen N03 for W05), as proposed in Fig.9 and Table 3. At the same time, a vertical pre-compressive load q was preliminarily applied to each log-wall specimen.

The typical deformed shape of each log-wall is shown in Fig. 10, while the comparison between numerical predictions and experimental results – in terms of horizontal in-plane load V versus top lateral displacement δ – is displayed in Fig.11. As shown, an excellent agreement was found for all specimens between the experimental curves and the numerical predictions. The accuracy and potential of the proposed numerical approach is further emphasized by the dissipation energy contributions listed in Table 4, where a percentage discrepancy Δ lower than 5% was found between experimentally and numerically estimated energies.

3.5. Parametric studies

Based on the preliminary experimental and numerical comparisons discussed in Section 3.4, further non-linear simulations were performed on different log-wall specimens, in order to properly assess the cyclic behaviour of *Blockhaus* structural systems having generic geometrical properties and subjected to in-plane lateral loads.

A first simple parametric investigation was performed by varying the width of specimen W01 from its original value (Table 1), in order to obtain a more representative model for real *Blockhaus* building. The dimensions of the analysed log-walls, subjected to a constant axial load (q= 10kN/m), were characterized in terms of uniform height (H_w= 2.91m) and variable width L_w (with L_w equal to 2.66m, 4m and 6m for the W01 log-wall and the parametric tests No.2-L or No.3-L respectively). Results obtained from this parametric study are displayed in Fig. 12a. As shown, the increase in the log-wall width resulted in higher axial loads in each spring, thus leading - in accordance with Eq.(3) - to wider hysteresis loops.

Starting from the original W01 specimen (L_w= 2.66m), the increase in dissipated energy for the 4m wall (No.2-L) is 42.8%, while for the 6m wall (No.3-L) is over 100%. This result is primarily due to friction effects, which give the largest dissipative contribution, as far as the small gaps present among the

intercepting logs allow possible sliding mechanisms. The same effects can be obtained by varying the friction coefficient or the pre-compressive axial load *q*; all these situations cause in fact a variation in the friction force given by Eq. (3), which linearly depends on the friction coefficient C_f and on the applied axial loads *N*. By keeping the original axial load of 10kN/m constant, the parametric test No.2-L gives the same results presented in Fig. 12a with a friction coefficient C_f= 0.6, and test No.3-L with a friction coefficient C_f= 0.9.

A second parametric study was also carried out to investigate the effects of variation in the height of the 'reference' log-wall W01. Three different height values H_w were taken into account (with H_w equal to 2.91m, 3.5m and 4.0m for the specimen W01 and the parametric tests No.2-H, No.3-H respectively) and the corresponding cyclic results are presented in Fig. 12b. As shown, a decrease in H_w causes a greater stiffness once the friction effect is finished due to the lower number of springs involved, but the effective energy dissipation remains the same.

3.6. Numerical analyses of *Blockhaus* log-walls with openings

Based on the geometrical configuration of specimen HW01, further numerical analyses were performed using the proposed FE-modelling approach on log-walls with openings such as a door and a window. An example is proposed in Fig. 13, where the deformed and undeformed shapes of the log-wall HW01 are displayed.

In accordance with the FE-model implementation and calibration of springs proposed in Sections 3.3-3.4, appropriate modifications were carried out, so that the nominal geometry and interaction among logs (e.g. near the openings) could be properly described.

At the lateral ends of the wall (Fig.13), specifically, the same spring calibration derived from the experimental cyclic test of the corner joint N01 (Fig.9a) was taken into account, since strictly related to (i) the log profile, (ii) the pre-compressive level and (iii) the joint typology.

Careful consideration was then given to the implementation of interrupted logs near the door and window openings. The metal profiles usually introduced along the vertical edges of the openings (e.g. Fig. 4) were fully neglected, since not rigidly connected to the adjacent timber logs. At the same time, appropriate springs

(type 'B' springs of Fig.13) were introduced along the vertical edges of door and window openings. These springs have the same axial stiffness described in Fig.9b and dynamic friction coefficient C_f= 0.408 (Fig.8 and Table 2), but null ultimate resistance under in-plane lateral loads, due to the lack of a physical mechanical joint. These springs, as a result, properly account for the capacity of this portion of logs to sustain the vertical compressive loads and, at the same time, to slide due to the applied in-plane lateral loads,

As previously discussed for log-walls W01-W05 without openings, numerical simulations performed on the log-wall HW01 resulted in a rather good agreement with the corresponding test results, in which a global failure mechanisms deriving from the collapse of logs between the door and window openings was noticed [9, 11]. Further validation of the presented simplified FE-model and on the predicted failure mechanism was carried out against a full 3D FE-model developed in accordance with [12]. Numerical and experimental comparisons are proposed in Fig. 14 in terms of measured in-plane shear V versus the top lateral displacement δ.

A percentage discrepancy in total energy contributions derived from experimental results and numerical predictions equal to -4.93% was found (Table 4). This analysis, as a result, confirmed the capacity of the presented modelling approach to properly simulate the cyclic behaviour of *Blockhaus* walls with openings, with the same level of accuracy previously highlighted for the specimens W01-W05 without openings (Table 4).

3.7. Comparison with 3D solid FE-models

Final comparative predictions were performed using the full 3D FE-models with solid elements presented in [12] and the simplified model discussed in this paper. A comparison among the monotonic response obtained from the full 3D solid model [12], the cyclic response predicted by the geometrically simplified model presented in this paper and the W01 experimental results is proposed in Fig. 15.

As shown, both the FE-models are able to properly simulate the structural behaviour of specimen W01 under in-plane lateral loads. However, the proposed simplified model has a significant advantage in terms of computational time: 140 beam elements and 620 DOFs for the simplified FE-model instead of 45,000 solid elements and 150,000 DOFs for the full 3D model.

Based on the good correlation among the simplified FE-models, the full 3D model and the full-scale experiments, it is thus expected that the simplified FE-model approach presented in this paper could be used to investigate the seismic vulnerability of whole *Blockhaus* buildings and structures.

4. Conclusions

In this paper, the structural behaviour of *Blockhaus* shear walls under in-pane lateral loads was investigated by means of an accurate yet computationally effective FE-model. The presented modelling approach uses rigid beams to schematize the logs, while non-linear springs acting in axial (vertical) and shear (horizontal) degrees of freedom describe the mechanical behaviour of corner joints between perpendicular walls. Unlike other simplified models presented in literature which needs calibration on experimental cyclic tests of full-scale *Blockhaus* walls, the main input parameters of the presented FE-model are represented by (i) the cyclic response of a single corner joint, as well as by (ii) the dynamic friction coefficient at the interface of the stacked timber logs in contact.

After an accurate calibration of the shear springs on the cyclic tests available for each type of *Blockhaus* corner joint, six full-scale log-walls were analysed using the proposed FE-model, by imposing them the same experimental displacement time-history derived from past quasi-static cyclic tests. The percentage discrepancy between experimental and numerical total energies of the examined log-walls was found to be less than 5%, hence demonstrating an excellent accuracy of the proposed modelling approach.

Two parametric studies, carried out by varying the width and the height of a reference full-scale specimen were also discussed. The first parametric analysis pointed out the linear dependency of the dissipated energy on the applied axial load, while the second parametric study (e.g. increase of the log-wall height) highlighted that the post-elastic stiffness of the whole subassembly decreases but the overall dissipative capacity remains the same. Finally, a further comparison with a full 3D solid modelling of a *Blockhaus* log-walls was presented, emphasizing the reduced computational burden of the proposed model and the rather good agreement between the obtained predictions, thus confirming the optimal level of accuracy provided by the presented FE-method.

Further experimental investigations – e.g. on whole *Blockhaus* buildings – are required to confirm the general validity of the presented FE-modelling assumptions. Based on the discussed comparisons, however, it is expected that the proposed FE-modelling approach could be further extended and used as practical but accurate tool for the investigation of the seismic behaviour and vulnerability of *Blockhaus* buildings.

Acknowledgments

Rubner Haus AG SpA is gratefully acknowledged for the financial and technical support. Dr. Annalisa Battisti (Rubner Haus), Dr. Roberto Tomasi (University of Trento) and Dr. Andrea Polastri (CNR Ivalsa) are also gratefully acknowledged for the technical support provided during the experimental investigations on full-scale *Blockhaus* timber walls and small carpentry joints.

References

[1] Rubner Haus AG SpA. www.haus.rubner.com

[2] Rusticasa, Construções Lda. www.rusticasa.pt

[3] T&B Log Homes, www.timberloghomes.co.za

[4] Wisconsin Log Homes Inc., http://www.wisconsinloghomes.com

[5] The Russian House®, www.russianloghouse.com

[6] Hirai, T., Kimura, T., Yanaga, K., Sasaki, Y., Koizumi, A. (2004). Lateral Resistance of Log Constructions, Proc. of the World Conference on Timber Engineering WCTE 2004, Volume III, pp.251-254.

[7] Branco, J., Araújo, J.P. (2010). Lateral Resistance of Log Timber Walls subjected to Horizontal Loads, Proc. of the World Conference on Timber Engineering WCTE 2010.

[8] Branco, J., Araújo, J.P. (2012). Structural behaviour of log timber walls under lateral in-plane loads, Engineering Structures, 40(3): 371-382.

[9] Giovannini, T., Grossi, P., Sartori, T., Tomasi, R. (2013). Blockhaus structural systems: full-scale experiments on shear walls [in Italian], University of Trento, Internal Technical Report.

[10] Tomasi, R., Sartori, T., Grossi, P., Wenzel, L. (2012). Blockhaus structural systems: experiments on carpentry joints [in Italian], University of Trento, Internal Technical Report.

[11] Giovannini T, Grossi P, Sartori T, Tomasi R (2014). Blockhaus system: experimental characterization of corner joints and shear walls. Proceedings of the World Conference on Timber Engineering WCTE2014, Quebec City, Canada, August 10-14.

[12] Bedon, C., Fragiacomo, M., Amadio, C., Sadoch, C. (2014). Experimental Study and Numerical Investigation of Blockhaus Shear Walls Subjected to In-Plan Seismic Loads, Journal of Structural Engineering 2014, DOI: 10.1061/(ASCE)ST.1943-541X.0001065.

[13] EN 338:2009. Structural timber-strength classes. European Committee for Standardisation, CEN, 2009, Brussels, Belgium.

[14] Bedon, C., Fragiacomo, M. (2015). Numerical and analytical assessment of the buckling behaviour of 'Blockhaus' log-walls under in-plane compression. Engineering Structures, 82: 144-150.

[15] Bedon, C., Rinaldin, G., Izzi, M., Fragiacomo, M., Amadio, C. (2015). Assessment of the structural stability of Blockhaus timber log-walls under in-plane compression via full-scale buckling experiments. Construction & Building Materials, 78: 474-490.

[16] EN 12512:2003. Timber structures - Test methods - Cyclic testing of joints made with mechanical fasteners. European Committee for Standardisation, CEN, 2009, Brussels, Belgium. UNI Italian translation.

[17] EN 1998-1:2004. Eurocode 8 - Design of Structures for Earthquake Resistance - Part 1: General rules, seismic actions and rules for buildings. European Committee for Standardisation, CEN, 2009, Brussels, Belgium.

[18] EN 1995-1-1:2009. Eurocode 5 - Design of timber structures - Part 1-1: General-common rules and rules for buildings. European Committee for Standardisation, CEN, 2009, Brussels, Belgium.

[19] Vogt, T., Hummel, J., Seim, W. (2012). Timber framed wall elements under cyclic loading, Proc. of the World Conference on Timber Engineering WCTE 2012, Auckland.

[20] Vasconcelos, G., Poletti, E., Salavessa, E., Jesus. A.M.P., Lourenço, P.B., Pilaon, P. (2013). In-plane shear behaviour of traditional timber walls, Engineering Structures, 56(5):1028–1048.

[21] http://www.roechling.it

[22] Simulia (2012). *ABAQUS v.6.*12 [Computer Software], Dassault Systems, Providence, RI, USA.

[23] Rinaldin, G., Amadio, C., Fragiacomo. M. (2012). A Component approach for the hysteretic behaviour of connections in cross-laminated wooden structures, Earthquake Engineering and Structural Dynamics, 42(13): 1885–2042, Wiley Online Library, DOI:10.1002/eqe.2310.

[24] Rinaldin, G. (2013). So.ph.i. software version 4.5, freely available at *http://giovanni.rinaldin.org*

Figure 1

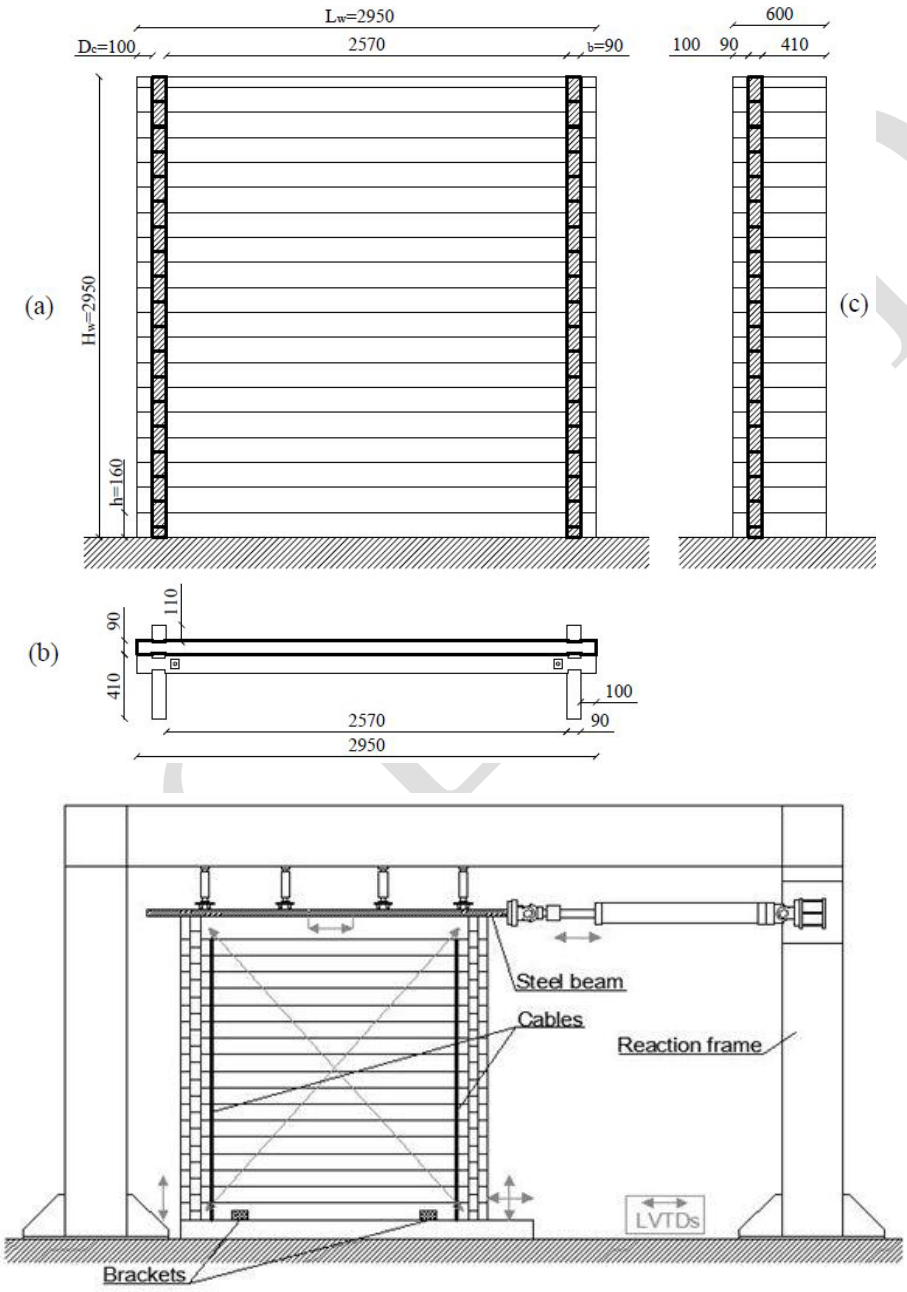

(d)

Fig. 1. Specimen W01: (a) elevation; (b) plan view; (c) lateral view (nominal dimensions in mm) and (d) experimental setup [12].

Figure 2

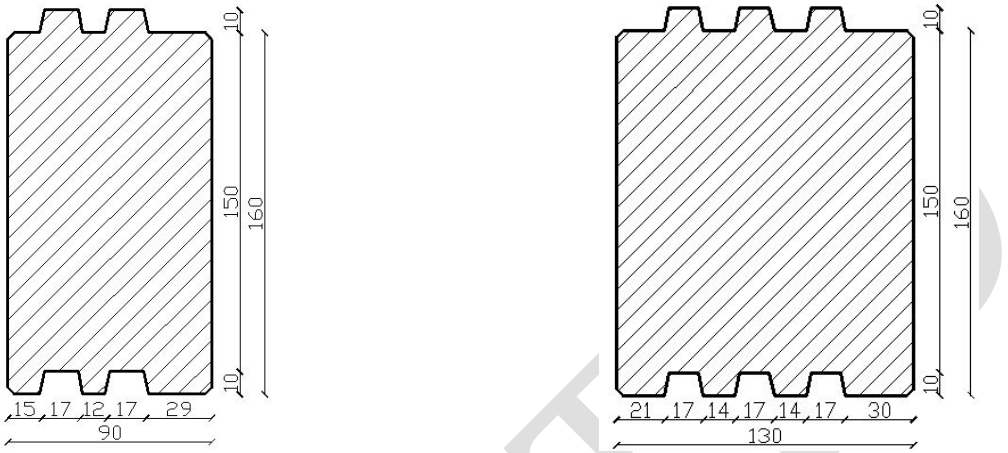

(a) (b)

Fig. 2. Cross-section of (a) 'Tirol' and (b) 'Schweiz' timber logs with tongues and grooves, nominal dimensions in mm [1].

Figure 3

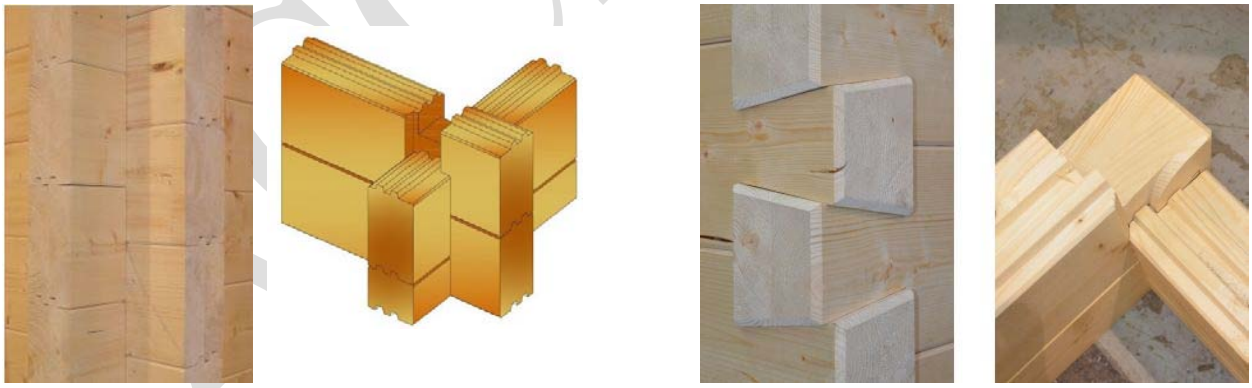

(a) (b)

Fig. 3. Corner joints of specimens. (a) 'Standard'; (b) 'Tirolerschloss' [1].

Figure 4

(a) (b) (c)

Fig. 4. Specimen HW01 [9]. (a) Overview and position of metal profiles; (b) Detail 1; (c) A-A' cross-section, nominal dimensions in mm.

Figure 5

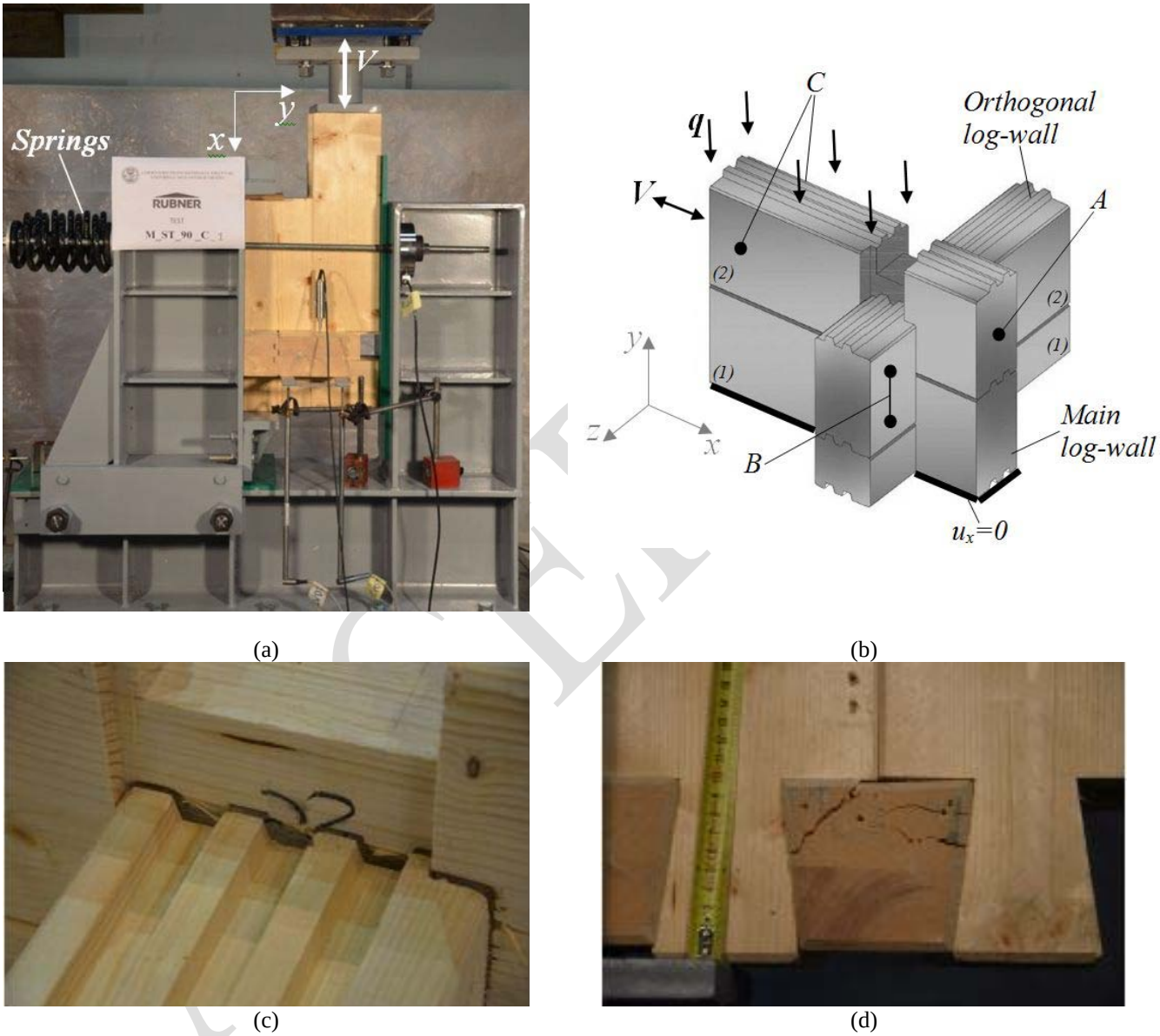

(a) (b)

(c) (d)

Fig. 5. Monotonic and cyclic experiments on *Blockhaus* corner joints [10, 11]. (a)(b) setup; (c) local crushing at the end of the experiment, specimen N02; (d) cracks in specimen N03 at the end of the experiment

Figure 6

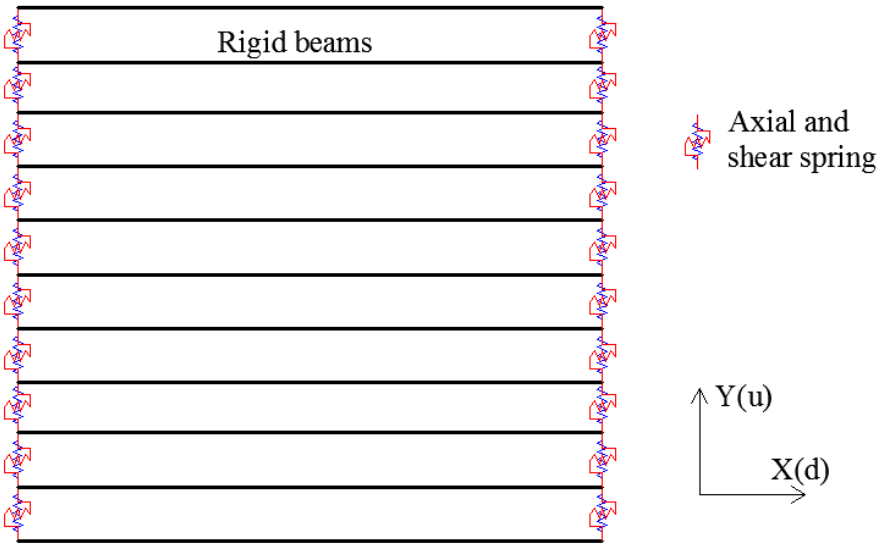

Fig. 6. Schematic of FE modelling adopted for the typical *Blockhaus* log-wall.

Figure 7

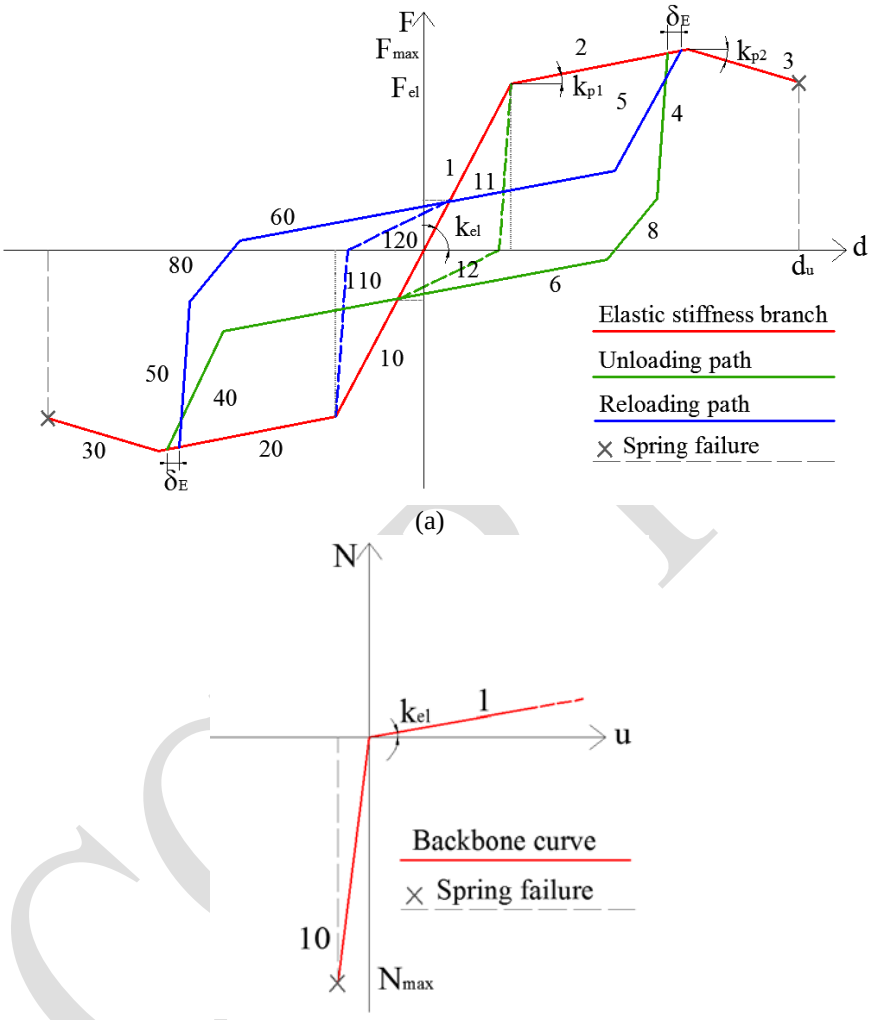

Fig. 7. Piece-wise hysteretic laws for (a) shear and (b) axial DOF.

1

2 # Figure 8

3

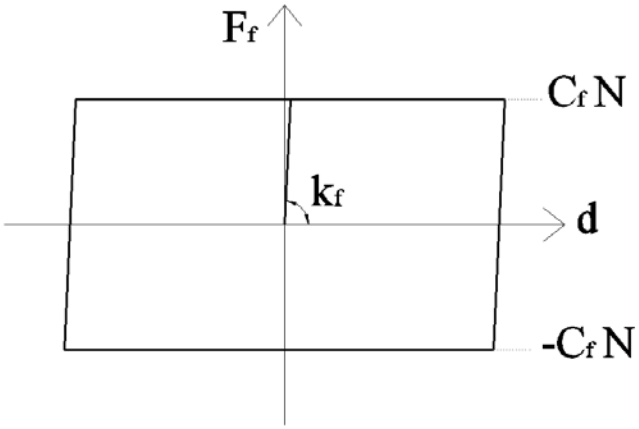

Fig.8. Constitutive relationship adopted for friction in the shear DOF of the spring.

4

5

Figure 9

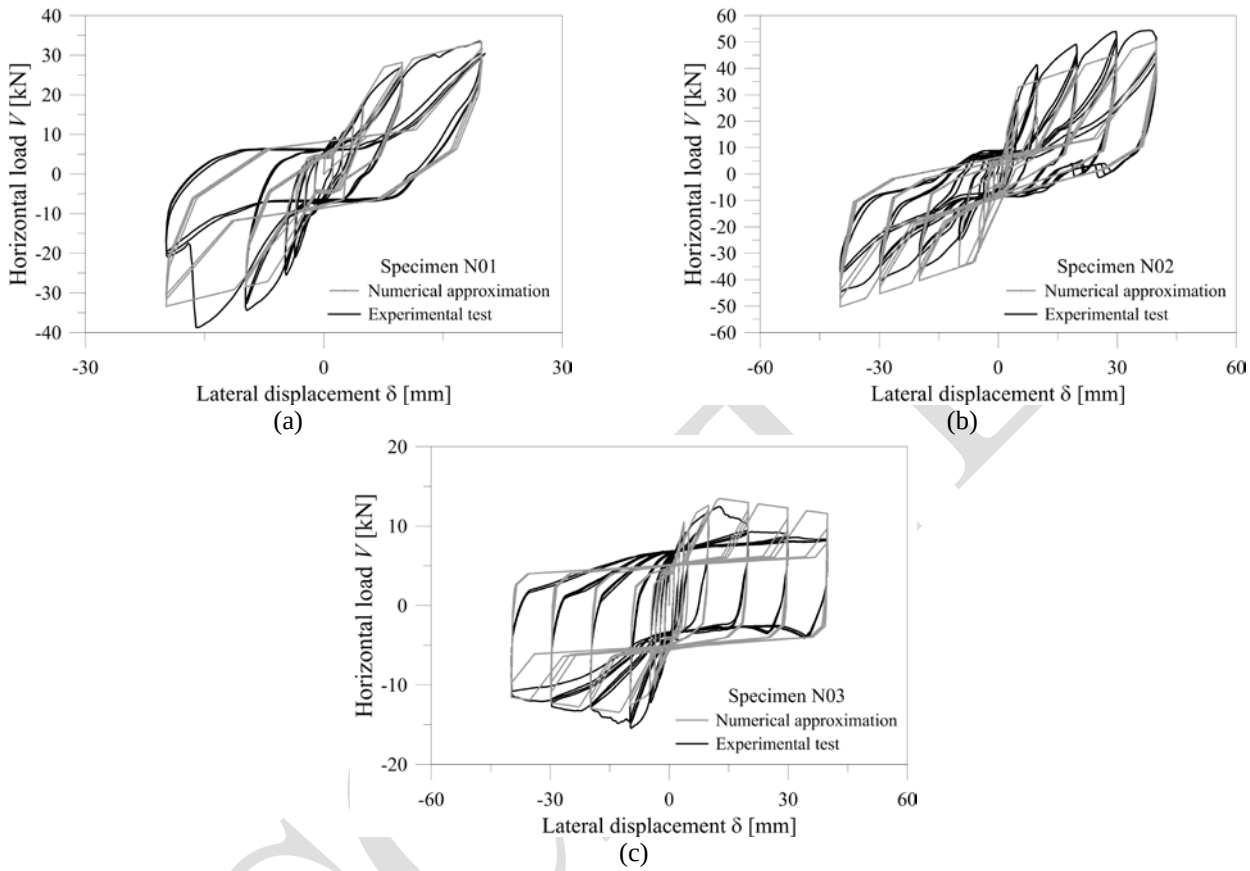

Fig. 9. Calibration of the shear DOF of the spring for each corner joint. Specimens (a) N01, (b) N02, (c) N03.

Figure 10

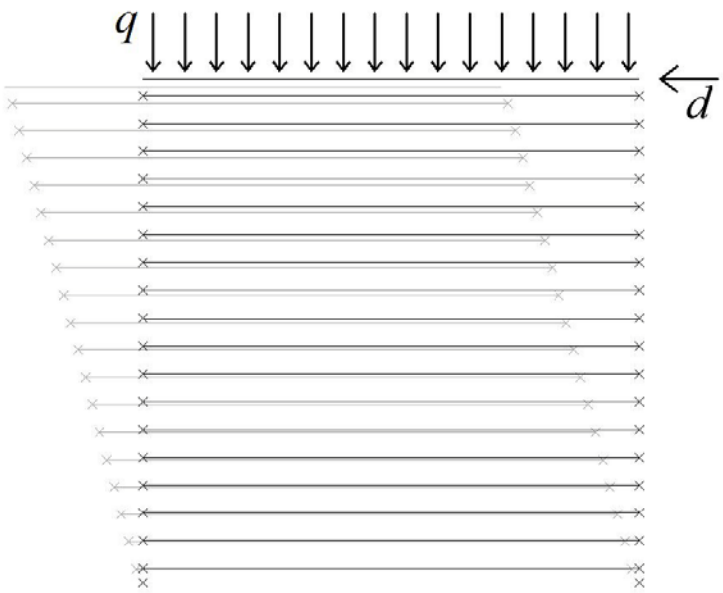

Fig. 10. Undeformed FE-model and typical deformed shaped (in grey, amplified 50 times in the horizontal direction, 500 times in the vertical direction). Springs are marked with a cross.

Figure 11

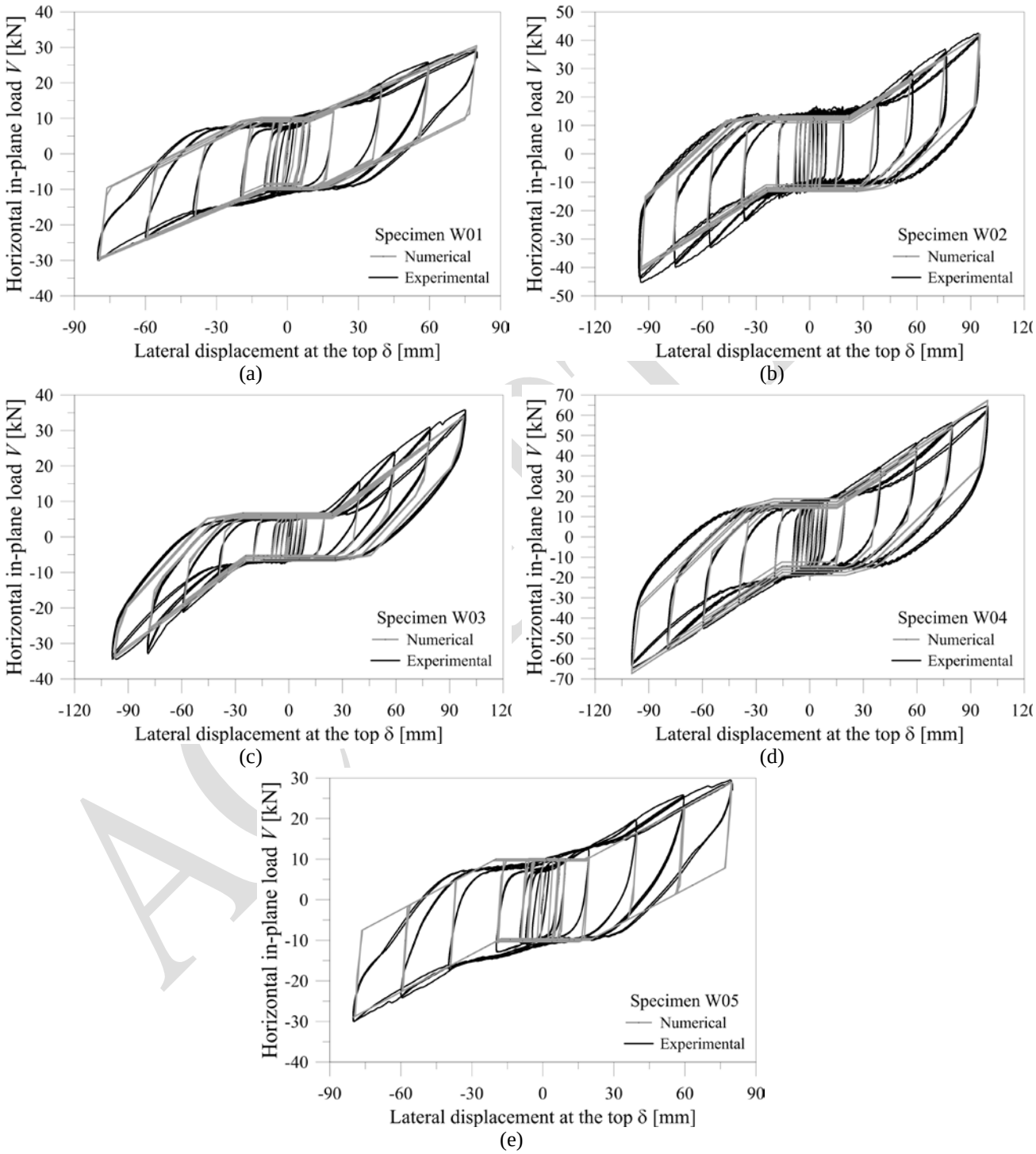

Fig. 11. Experimental-numerical comparison for specimens (a) W01; (b) W02; (c) W03; (d) W04; (e) W05.

1

2 **Figure 12**

3

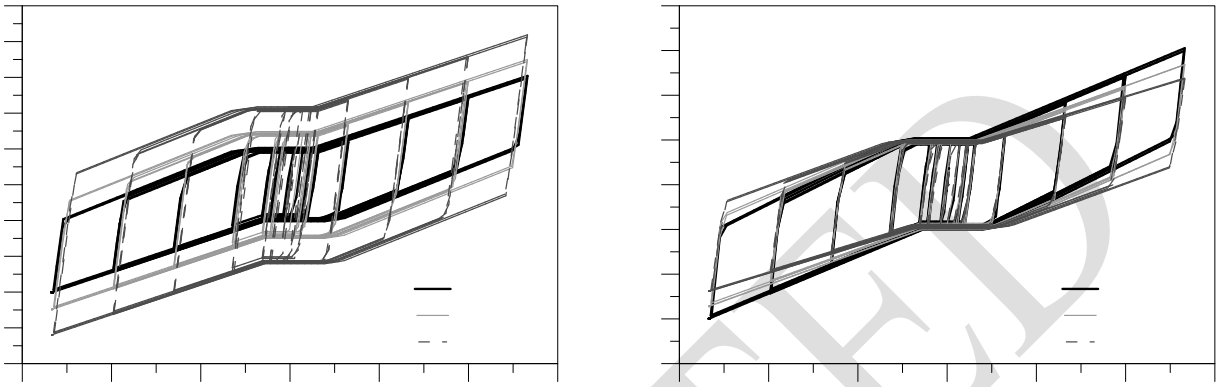

(a) (b)

Fig. 12. Horizontal in-plane load V vs. lateral top displacement δ for Specimen W01, by varying the log-wall (a) width or (b) height.

4

5 **Figure 13**

6

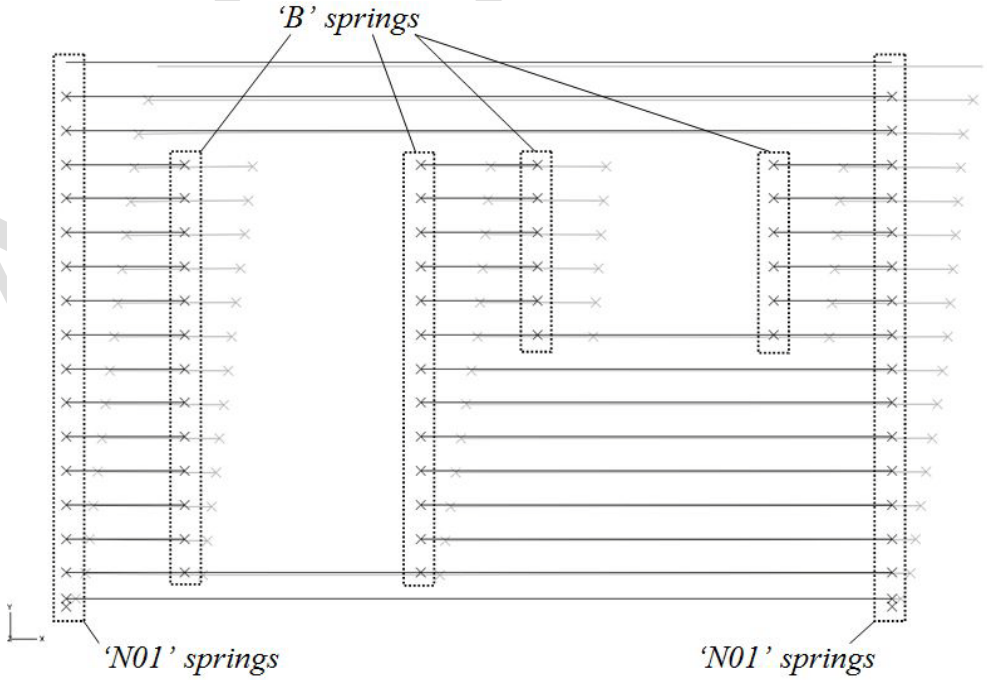

Fig. 13. Undeformed (in black) and typical deformed shape (in grey, amplified 50 times in the horizontal direction, 500 times in the vertical direction) of the wall specimen HW01. Springs are marked with a cross.

Figure 14

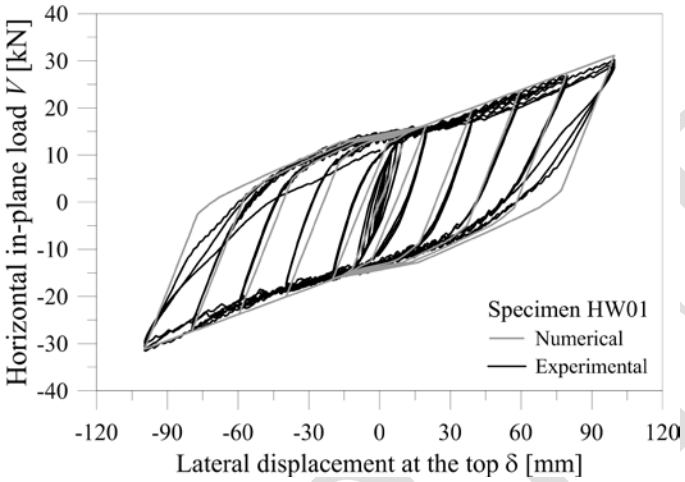

Fig. 14. Experimental-numerical comparison in terms of total base shear vs. lateral top displacement for specimen HW01.

Figure 15

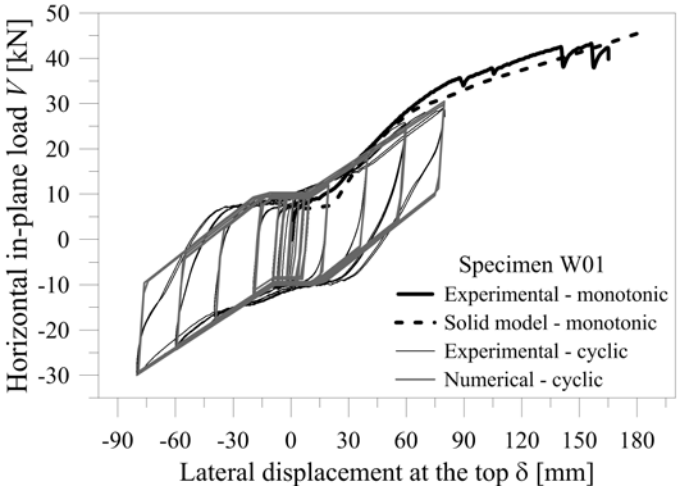

Fig. 15. Experimental-numerical comparison in terms of total base shear vs. top displacement for the specimen W01.

Table 1

Table 1. Geometrical properties of full-scale *Blockhaus* specimens and results obtained from cyclic experiments [9, 12]. S: 'Standard' joint; T: 'Tiroloerschloss' joint. δ_{max}: maximum lateral displacement; V_{max}: maximum shear load; V_k: maximum expected characteristic shear load (with 'c' or 's' signifying a compressive or shearing failure mechanisms, Eqs.(1a)-(1b)).

Specimen #	Geometry									Test results		
	Main log-wall					Corner joint		Openings	Precompression			
	Height H_w [m]	Length L_w [m]	Widt h b [m]	Section type [-]	Number of logs [-]	Type [-]	Distance D_c [m]	[-]	q [kN/m]	δ_{max} [mm]	V_{max} [kN]	V_k [kN]
W01	2.96	2.95	0.09	Tirol	18 + ½	S	0.1	No	10	80	30.0	33.0 *c*
W02	2.80	3.91	0.09	Tirol	17 + ½	S	0.1	No	10	100	45.2	33.0 *c*
W03	2.80	2.50	0.09	Tirol	17 + ½	S	0.1	No	5	100	35.8	33.0 *c*
W04	2.80	3.91	0.13	Schweiz	17 + ½	S	0.1	No	10	100	64.7	42.1 *c*
W05	2.96	2.95	0.09	Tirol	18 + ½	T	0.0	No	10	80	18.5	14.4 *s*
HW01	2.80	3.91	0.09	Tirol	17 + ½	S	0.1	Door + window	10	100	31.5	33.0 *c*

Table 2

Table 2. Equivalent damping ratios ν_{eq} at different lateral displacements δ (first full cycle) and friction coefficient μ obtained from full-scale cyclic experiments.

Specimen #	Imposed lateral displacement δ [mm]					μ
	20	*40*	*60*	*80*	*100*	
W01	0.061	0.082	0.107	0.129	-	0.382
W02	0.053	0.079	0.088	0.103	0.118	0.344
W03	0.051	0.107	0.145	0.161	0.178	0.525
W04	0.059	0.080	0.099	0.116	0.124	0.485
W05	0.059	0.079	0.104	0.125	-	0.345
HW01	0.074	0.074	0.088	0.102	0.115	0.364
Average	*0.060*	*0.084*	*0.105*	*0.123*	*0.140*	*0.408*

Table 3

Table 3. Parameters obtained from calibration of the approximated model on the experimental results of each corner joint.

Parameter		Specimen #			Units
Symbol	Description	N01	N02	N03	
k_{el}	*Elastic stiffness*	3.34	5.67	2.25	kN/mm
F_{el}	*Force at elastic limit*	23.01	28.96	6.50	kN
k_{p1}	*First inelastic stiffness*	0.49	0.50	0.30	kN/mm
F_{max}	*Maximum strength*	33.51	54.37	9.45	kN
k_{p2}	*Second inelastic stiffness*	-1.47	-1.50	-0.07	kN/mm
k_{sc}	*Stiffness factor for unloading branch*	1.5	1.35	2	-
R_C	*Strength ratio of reloading branch*	0.6	0.6	0.7	-
S_C	*Strength ratio of unloading branch*	0.65	0.68	0.8	-
d_u	*Ultimate displacement*	20	40	40	mm
k_{deg}	*Stiffness degradation factor*	0.6	0.6	0.6	-
α	*Strength degradation parameter*	1	1	1	-
γ	*Strength degradation parameter*	0.0003	0.0002	0.0005	-
Gap	*Gap opening*	1	1	1	mm
k_5	*Stiffness factor for branches #5 and #40*	1.2	0.65	0.5	-

Table 4

Table 4. Differences on total energy for the tested corner joints and full-scale log-walls.
$\Delta = 100 \cdot \left(E_{\exp} - E_{num} \right) / E_{num}$.

Specimen #	E_{exp} [kNmm]	E_{num} [kNmm]	Δ [%]
N01	3.48	3.37	3.26
N02	10.92	10.98	-0.55
N03	6.82	6.71	1.64
W01	22.06	22.6	-2.39
W02	47.51	45.46	4.51
W03	22.84	23.74	-3.79
W04	65.22	63.04	3.46
W05	22.06	23.17	-4.79
HW01	36.14	38.42	-4.92